

Brightening of dark trions in monolayer WS₂ via localization of surface plasmons

Sreyan Raha,^{1,*} Tara Shankar Bhattacharya,^{1,2} Indrani Bose,¹ and Achintya Singha^{1,†}

¹*Department of Physical Sciences, Bose Institute,*

EN 80, Sector V, Bidhannagar, Kolkata 700091, India.

²*Kolaghat Government Polytechnic, Kolaghat 721134, India.*

Among all excitonic complexes in transition-metal dichalcogenides (TMDs), dark and semi-dark trions are poised to play a stellar role in future quantum technologies due to their long lifetimes, about two orders of magnitude greater than those of their bright counterparts. In monolayer (ML) tungsten disulphide (WS₂), accessing these states via a suitable brightening mechanism remains challenging, specially, at elevated temperatures. Here, we demonstrate the brightening of dark trions from ML WS₂ over the temperature range, 83 K–115 K, enabled by localized surface plasmon modes in a disordered gold substrate. The resulting photoluminescence (PL) spectrum reveals a distinct spectral doublet with the twin peaks of semi-dark and bright trion states, separated by ~ 45 meV. The origin of the semi-dark trion state lies in intervalley electron-electron scatterings, while its visibility in the PL spectrum is made possible by the enhanced out-of-plane electromagnetic field associated with plasmon localization. We also report on the negative degree of circular polarization in ML WS₂ at the energy of the semi-dark trion state. Our results establish a scalable plasmonic route to access valley-polarized semi-dark trions, opening new opportunities for quantum and valleytronic applications.

arXiv:2512.10856v2 [cond-mat.mes-hall] 24 Jan 2026

* Present Address : Univ Toulouse, INSA Toulouse, CNRS, LPCNO, Toulouse, France.

† Corresponding author: achintya@jcbose.ac.in

I. INTRODUCTION

Monolayer (ML) transition metal dichalcogenides (TMDs) represent a distinctive class of atomically thin semiconductors known for their remarkable exciton dynamics and spin-valley coupled properties. The characteristic features of the ML materials allow for a number of unique physical properties [1, 2]. A direct band gap separates the lowest conduction band (CB) and the highest valence band (VB) states at the $\pm K$ valleys of the electronic band structure. Coulomb interaction along with reduced dielectric screening facilitate the formation of an optically generated exciton, a bound pair of an electron and a hole, across the gap. A combination of broken inversion symmetry and time-reversal symmetry (degenerate energy states with opposite spin orientations) of the band states at the $\pm K$ valleys give rise to observable valley-specific phenomena, e.g., valley-selective optical excitation with circularly polarized light [1, 2]. Additionally, the presence of strong spin-orbit coupling splits the VB and CB states with the splitting magnitude much larger in the case of the VB. The spin splitting of the band states couples the spin and valley degrees of freedom and allows for the formation of excitonic complexes like dark excitons and dark/bright triions. These attractive features, taken together, are central to emerging valleytronic applications in optoelectronics, spintronics and quantum information-based technologies.

While bright excitons in ML TMDs have been extensively investigated, increasing attention is now devoted to their dark counterparts, particularly in tungsten-based materials such as WS_2 and WSe_2 [3–7]. In these systems, the lowest-energy exciton turns out to be an optically inactive dark exciton with the spins of the associated CB and VB states being antiparallel. The dark state is populated via the thermal relaxation of an optically generated bright exciton to the lower energy state. The negatively charged triions in ML TMDs, which are bound complexes of two electrons and a hole, are of three types: bright intravalley or singlet triion (X_S^-) with the optically generated bright exciton and a bound resident electron located in the same valley, bright intervalley or triplet triion (X_T^-) and the dark triion (X_D^-), as depicted in Figs. 1(a–c). Owing to its charged three-particle structure, a triion encodes more information than a single electron with the added advantage that some of its properties are electrically tunable. The lifetime of an excitonic complex is finite due to both radiative and non-radiative decay processes. Since a dark triion, being optically inactive, does not undergo radiative decay, its lifetime is about two orders of magnitude larger than that of a bright triion, making it a promising candidate for optoelectronic and quantum information applications [8, 9].

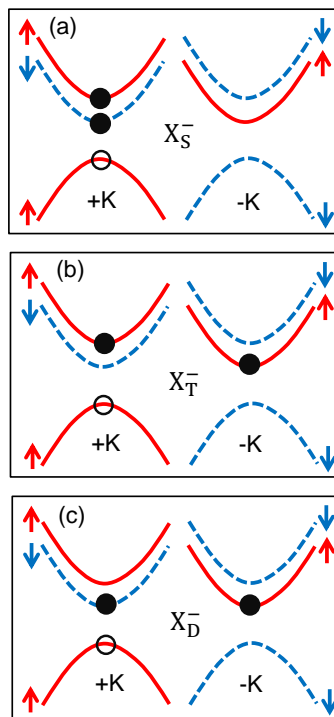


FIG. 1. (a) singlet bright triion (X_S^-), (b) triplet bright triion (X_T^-), (c) dark triion (X_D^-).

Such applications, however, require at least a partial optical activation (“brightening”) of the dark excitonic complexes for their detection. Various approaches have been explored so far to achieve the brightening, e.g, by using

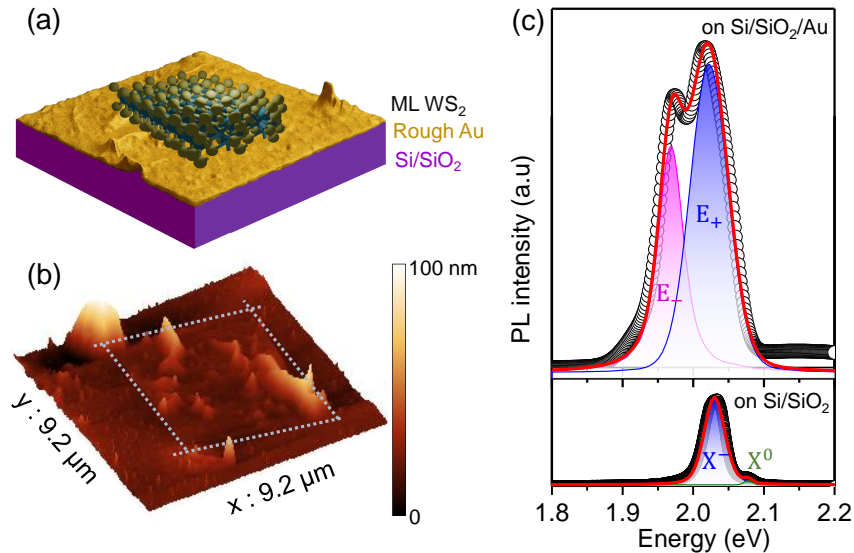


FIG. 2. (a) A schematic diagram of the experimental arrangement of the ML WS₂ sample on a disordered Au film with an underlying Si/SiO₂ substrate. (b) A 3D AFM profile of the rough gold surface with the sample covering the dotted rectangular area. (c) PL spectra at T= 83 K of ML WS₂ placed on the Si/SiO₂ substrate (colored blue), and on the Si/SiO₂/Au substrate (colored red).

magnetic fields, through strain engineering and via coupling to nanostructures with enhanced light-matter interactions [3–5, 8, 10–12]. Though a number of studies have been carried out on the brightening of dark excitons and trions in ML WSe₂ over an extended temperature range, the situation is markedly different for ML WS₂ [10].

In this paper, we report on the optical activation of the dark trion state in ML WS₂ at elevated temperatures (83 K–115 K) by exploiting Anderson-like localization of surface plasmons in a disordered Au film in contact with the TMD ML [13, 14]. Through temperature-dependent photoluminescence (PL) spectroscopy, we identify a distinct spectral doublet in the temperature range of 83 K–115 K, with the lower and higher energy peaks attributed to the semi-dark trion ($|E_{-}\rangle$) and bright trions ($|E_{+}\rangle$), respectively. A theoretical model [15] suggests the semi-dark trion state ($|E_{-}\rangle$) to be a mixed state of the dark ($|D\rangle$) and bright trion ($|B\rangle$) states coupled via electron-electron (e-e) intervalley scatterings. The Anderson-like localized surface plasmons in the disordered Au film contribute to the optical brightening of the dark trions and also in the enhancement of the PL signals from bright trions. Using polarization-resolved PL spectroscopy, we further show that the degree of circular polarization (P_c) is negative at the peak energy of the semi-dark trion state ($|E_{-}\rangle$). Our findings provide the experimental evidence of the brightening of dark trions in ML WS₂ above cryogenic temperatures and establishes a scalable strategy for accessing spin-forbidden states in TMDs.

II. RESULTS AND DISCUSSIONS

Figure 2(a) schematically shows the WS₂ ML deposited on a disordered Au film supported by a Si/SiO₂ substrate. See Section I of supporting information for the details of the sample preparation. The incident laser excites collective oscillations of free electrons in the Au surface generating surface plasmons. The structural disorder in the Au film gives rise to Anderson-like localization of these modes in the form of localized surface plasmons (LSPs) [13, 14]. Figure 1(b) exhibits a 3D AFM image of the rough gold surface, with the region enclosed by the white dotted line indicating the area covered by the WS₂ ML.

Fig. 2(c) compares the PL spectra at 83 K of the ML WS₂ sample on Si/SiO₂, with and without the intervening Au film. While the PL emission spectrum of ML WS₂ on the Si/SiO₂ substrate has contributions from both bright excitons (X⁰) and negatively-charged bright trions (X⁻) [Fig. S1(a)], the presence of the rough Au substrate gives rise to a substantial electron doping of the ML due to charge transfer from Au [16], resulting in the neutral exciton population becoming negligible as the temperature is lowered, with most of the excitons effectively converted into trions [Fig. 2(c)] [17]. This allows one to exclusively focus on the dynamics of the trions. In the presence of the Au film, a notable PL enhancement is observed, consistent with plasmon-assisted emission [17–21]. Most importantly,

the rough Au substrate gives rise to a distinct PL doublet with a peak separation of about 45 meV.

To exclude localized strain as the origin of the new spectral feature, we performed spatially resolved PL measurements across different regions of the sample. As shown in Fig. 3(a), the spectral shape remains uniform across the entire sample along the line 1–5. We have also carried out position-dependent Raman measurements, described in Section III of the Supporting Information, and probed the local topography using AFM (Section IV, Supporting Information) to confirm that the observed optical response of the sample is not strain-induced.

We further examined the nature of the two peaks through laser power-dependent PL measurements at 83 K with the spectra shown in Fig. S4. The log-log plot of the integrated PL intensity, I versus the laser power, P [Fig. 3(b)] reveals a linear relationship, $I \propto P^k$, with $k \sim 1.2$ (~ 1) for the higher (lower) energy peak, ruling out emissions due to defect-bound recombination processes which typically show sub-linear scaling ($k < 1$) [22].

In ML TMDs, bright excitons and trions have in-plane (IP) dipole moments, while dark excitons and trions carry out-of-plane (OUP) dipole moments. In standard optical set-ups for probing circularly polarized PL, light is incident along a direction normal to the sample so that the associated electric field is IP. As per Fermi’s Golden Rule (FGR), the radiative transition, i.e., the PL emission rate is proportional to $|\mathbf{p} \cdot \mathbf{E}|^2$ where \mathbf{p} is the electric dipole moment of the emitter (exciton/trion) and \mathbf{E} the optical electric field vector so that only the bright excitons and trions are optically active. As discussed by Purcell [4], the spontaneous emission rate of a quantum emitter is considerably enhanced in a confined electromagnetic environment provided by nanostructures. Such an environment provides a large density of available electromagnetic states for the quantum emitter to emit into, raising the emission rate considerably. In the light of the above discussion, we now elucidate the role of the rough Au film in the generation of an enhanced PL signal. The LSPs generated in the rough Au film have a prominent OUP electric field pointing in the z-direction. This is demonstrated in Fig. S5(b), through numerical simulations of the electric field intensity, ($|E_z|^2$), associated with the LSPs. The figure displays localized hot spots of high field intensity, above the experimentally measured AFM topography, with an enhancement factor in the range of 100-200. The OUP electric field couples to the OUP dipole moment of the dark trion enabling a radiative transition (the factor $|\mathbf{p} \cdot \mathbf{E}|^2$ in FGR) and hence the “brightening” of the dark trion. The Anderson-type localization of the surface plasmons in the Au film gives rise to enhanced near-fields as well as an increased local density of states (LDOS) (the Purcell effect) giving rise to a marked enhancement of the PL signal. Furthermore, the less dominant IP components of the plasmonic field couple to the IP electric dipole moments of the bright trions so that the PL emission from the bright trions is also enhanced [23]. The brightening of the negatively-charged dark trion with detectable intensity necessitates the doping of the sample with electrons so that the process of trion formation becomes favorable [24]. A doped electron lowers its energy by binding to an exciton and forming thereby a trion. In our experiment, the doping is predominantly mediated via the Au film, which also provides the plasmonic environment for enhanced PL signals, so that in its absence the PL signal from the bright trion is much diminished in intensity [Fig. 2(c)].

The two PL peak energies of the spectral doublet [Fig. 2(c)], denoted by E_- and E_+ with $E_- < E_+$, correspond to mixed states of dark ($|D\rangle$) and bright ($|B\rangle$) trions. A two-component analysis of the spectrum [Fig. 2(c)] reveals a substantial spectral overlap of the components. The coupled state with energy E_- (E_+) has the dark (bright) trion as the dominant component and can be characterized as a semi-dark ($|E_- \rangle$) (bright ($|E_+ \rangle$)) trion state. To investigate the temperature dependence of the peak intensities, PL measurements were performed from 83 K to 293 K. The false color map of normalized PL intensity in Fig. 3(c) shows the emergence of E_- near 115 K, while Fig. 3(d) shows the integrated intensities of both the peaks as a function of temperature. The semi-dark trion ($|E_- \rangle$), being the lower energy state, does not require thermal activation and its PL intensity is expected to be higher than that of the bright trion at low temperatures. On the other hand, the bright states are dominant at elevated temperatures due to thermal activation from the dark states. This thermal behavior can be modeled in the framework of a two-level system by the following equation based on the Boltzmann distribution:

$$I(T) = A \frac{e^{(-\frac{\Delta E}{k_B T})}}{1 + e^{(-\frac{\Delta E}{k_B T})}} + B, \quad (1)$$

where $I(T)$ is the PL intensity of the E_+ peak, A is a proportionality constant, B is a temperature-independent background term, k_B is the Boltzmann constant, and ΔE the energy separation between the two states. As shown in the inset of Fig. 3(d), the model provides a reasonable fit to the experimental data in the 83–115 K range. The extracted value of $\Delta E \sim 42 (\pm 5)$ meV is consistent with the experimentally observed energy separation between the two components of the doublet. The ascending part of the bright trion ($|E_+ \rangle$) plot reflects the plasmonic enhancement of the PL intensity while the descending part indicates the thermal breakup of the trions. At $T \sim 113$ K, the PL intensity of the E_+ peak is enhanced by a factor of ~ 5 from the value obtained in the case of ML WS₂ on a Si/SiO₂ substrate. In the absence of the Au component of the substrate, the bright trion peak dominated the PL spectrum and that too with much diminished intensity [Fig. 2(c)]. The PL intensity of this bright trion decreases with increasing temperature (Fig. S7).

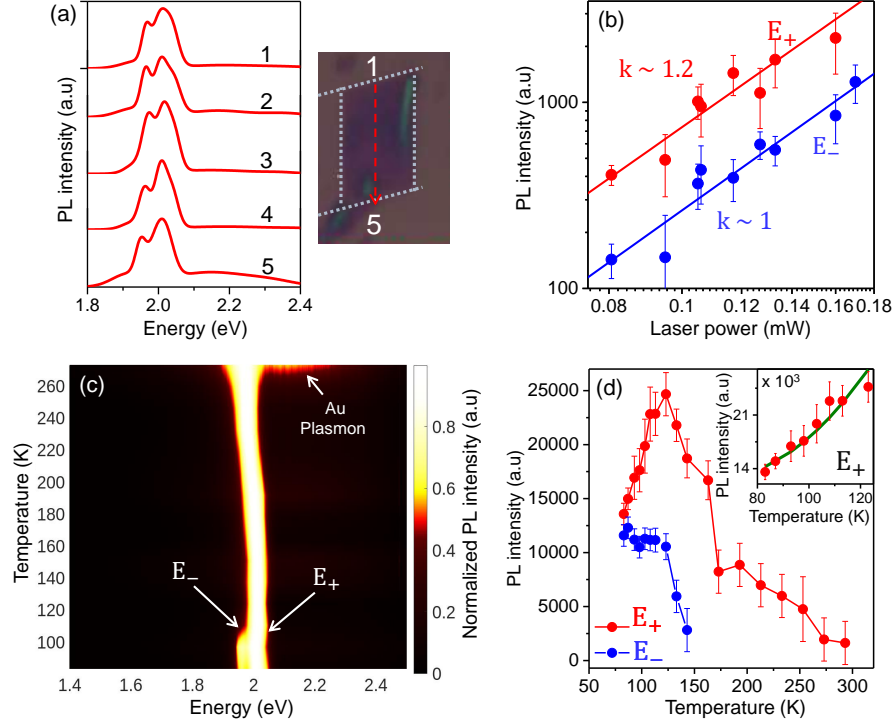


FIG. 3. (a) PL spectra at 83 K from different regions of the sample, along the line shown in the right panel. (b) PL integrated intensity of E_+ and E_- peaks at 83 K as a function of laser power. (c) False color plot for normalized PL intensity as a function of temperature from ML WS₂ on rough Si/SiO₂/Au substrate. (d) Integrated PL intensity of E_+ and E_- states as a function of temperature.

As discussed previously, it is likely that the observed doublet in the PL emission spectrum originates from the mixing of the dark ($|D\rangle$) and bright ($|B\rangle$) trion states. In the theoretical model proposed by Danovich et al. [15], the mixing is brought about by intervalley electron-electron (e-e) scatterings which convert the dark trions ($|D\rangle$) into brightened semi-dark (gray) [$|E_-\rangle$] ones. Fig. 4 (a) shows a schematic diagram of the intervalley e-e scattering in which two electrons occupying the lower CB subbands at the $\pm K$ valleys, constituting X_D^- , are scattered to the upper CB subbands of the opposite $\pm K$ valleys resulting in the formation of an excited bright trion configuration (the upper subband of each valley occupied by an electron). The dark trion $|D\rangle$ and bright trion $|B\rangle$ states are described by the valley and spin configurations $|D\rangle \equiv |T_{\downarrow+K, \uparrow-K}^{\uparrow+K}\rangle$ and $|B\rangle \equiv |T_{\uparrow+K, \downarrow-K}^{\uparrow+K}\rangle$, respectively [Fig. 4(a)]. The optical recombination of the e-h pair in the $+K$ valley results in the experimentally observed PL emission corresponding to the semi-dark trion. Due to the requirement of energy conservation, the light emission energy from the semi-dark trion is shifted by an energy equal to the CB spin-orbit splitting, Δ_{SO} , from the energy of X_D^- , i.e. $E_- = E_{D^-} - \Delta_{SO}$. The observation of the X_D^- emission line has been reported for both WS₂, WSe₂ samples through the brightening of the dark trion by a magnetic field [6, 25, 26]. In all the reported experiments, the semi-dark trion emission line is seen at a lower energy with the energy shift given approximately by 12 meV, suggesting a similar value for Δ_{SO} .

There is now considerable experimental evidence for the formation of semi-dark trion state via intervalley e-e scattering [25–27]. The PL spectra were obtained at low temperatures, e.g., at 5 K [25] and 7 K [26] for the ML WS₂ sample. Similar low temperature PL measurements were carried out for the ML WSe₂ sample [27]. In this case, the substrate used was Si/SiO₂ and the required doping was achieved via electrostatic gating. The emission signal from the semi-dark trion, formed via intervalley e-e scattering, was prominently visible in the PL spectrum only at low temperatures and lost visibility around 60 K. In the case of the ML WS₂ sample also, the detection of the semi-dark trion peak in the PL spectrum could be achieved only at very low temperatures. The significant loss in intensity at elevated temperatures is due to the thermal activation of the trions from the semi-dark to the bright state. The inclusion of the rough Au film, in our substrate, extends the temperature range for the detection of the semi-dark trion, via the LSP-mediated amplification of the weak signal. Apart from amplifying the PL signals from both the semi-dark and bright trions, the plasmonic coupling, additionally, brings about the brightening of the dark trion. In the earlier experiments, the brightening was achieved with a magnetic field [6, 25]. In some of these experiments [6, 25, 26], four trion peaks could be resolved in the PL spectrum, associated successively with the semi-dark (lowest

energy), dark [Fig. 1(c)], bright singlet and triplet [Figs. 1(a) and (b)] trions. The dark trion acquires visibility in the PL spectrum due to magnetic-field brightening. On the other hand, the semi-dark trion, formed via intervalley e-e scattering, is detected in the absence of a magnetic field [25]. Our PL measurements on ML WS₂, with an underlying disordered Au film/Si/SiO₂ substrate, were carried out at elevated temperatures with the PL spectrum displaying only a doublet [Fig. 2(c)]. A four-component analysis of the doublet at 83 K (Fig. S8) shows overlapped PL signals from all the four trions with successive peak positions at 1.9691 eV, 1.9831 eV, 2.0148 eV and 2.0278 eV. These energies are red-shifted from the corresponding peak positions at 1.996 eV, 2.0078 eV, 2.028 eV and 2.034 eV, as reported in [26] at 7 K. The peak energy difference between the dark and semi-dark trions, in our analysis of the PL signal, is obtained as 14 meV, close to the estimates reported earlier [6, 25–27]. The splitting energy between the triplet and singlet trions is approximately 13 meV. Based on a similar component analysis, a value of 11 meV has been obtained for ML WS₂ [28].

As proposed by Danovich et al. [15], the bright ($|B\rangle$) and dark trion ($|D\rangle$) states in a monolayer sample are coupled through intervalley e-e scatterings giving rise to two mixed states, a semi-dark trion state ($|E_-\rangle$) and a state similar to the bright trion state ($|E_+\rangle$). The coupling can be described by a 2×2 matrix

$$H = \begin{pmatrix} E_b & \mu \\ \mu^* & E_d \end{pmatrix}, \quad (2)$$

in the basis states $|B\rangle$ and $|D\rangle$ representing the bright and dark trion states with respective energies E_b and E_d with μ being the coupling parameter. The energies E_{\pm} of the higher and lower peak positions [Fig. 2(c)] are given by

$$E_{\pm} = \frac{E_b + E_d}{2} \pm \frac{1}{2} \sqrt{(E_b - E_d)^2 + 4|\mu|^2}$$

with the corresponding state vectors given by $|E_+\rangle$ and $|E_-\rangle$ respectively. The dominant (minority) component of the semi-dark trion state $|E_-\rangle$ is the dark (bright) trion state. The reverse is true for the bright trion state $|E_+\rangle$. Due to the presence of LSPs in the plasmonic Au substrate, the PL emission intensity gets enhanced for both the trion states. The energy gap between the two peaks is given by

$$\Delta_D = E_+ - E_- = \sqrt{(E_b - E_d)^2 + 4|\mu|^2} = \sqrt{(2\Delta_{SO})^2 + 4|\mu|^2}$$

where $E_b - E_d \approx 2\Delta_{SO}$ and Δ_{SO} is the spin-orbit splitting of the conduction band. Single-particle estimates, extracted from magneto optical spectroscopy and transport measurements, yield $\Delta_{SO} = 12 \pm 1$ meV for WS₂ and $\Delta_{SO} = 12 \pm 0.5$ meV for WSe₂ [29, 30]. These values are notably smaller than those from band-structure calculations (e.g., $\Delta_{SO} = 32$ meV for WS₂ [15]), but are in agreement with the estimates inferred from the peak energy differences of brightened dark and semi-dark trions in the PL spectra of the previously reported experiments [6, 25, 26]. The coupling parameter μ has been calculated as $\mu = 18$ meV for WS₂ MLs [15]. Using $\Delta_{SO} = 12$ meV and $\mu = 18$ meV in Eq. (3), one obtains $\Delta_D = 43.3$ meV, in close agreement with the experimentally observed value of $\Delta_D = 45$ meV. Taking $\Delta_{SO} = 13$ meV (within the experimental uncertainty) gives $\Delta_D \approx 44.4$ meV. The quantitative analysis firmly links the observed PL spectral doublet [Fig. 2(c)] to coupled dark and bright trion states, with the extracted peak energy splitting in good agreement with the theoretical estimate based on intervalley e-e scattering. A similar agreement between theoretical and experimental estimates of Δ_D has been demonstrated in the case of ML WSe₂ [27]. At this point, we emphasize that while intervalley e-e scatterings govern the formation of the mixed trion states, ($|E_-\rangle$) and ($|E_+\rangle$), the PL emission intensity depends on the coupling between the electric dipole moment of the emitter and the plasmonic near-field, the electromagnetic environment (Purcell effect) as well as the temperature.

To probe the valley dynamics of the trion states, we performed circular polarization-resolved PL measurements. The sample was excited with $\sigma+$ light, and the PL signals were detected in the $\sigma+$ and $\sigma-$ detection channels. The degree of circular polarization, P_c , is calculated as

$$P_c = \frac{I(\sigma+) - I(\sigma-)}{I(\sigma+) + I(\sigma-)}, \quad (3)$$

where $I(\sigma+)$ and $I(\sigma-)$ correspond to the intensity of the PL signal detected in the $\sigma+$ and $\sigma-$ channels, respectively. The P_c (magenta curve) as a function of energy, shown in Fig. 4(b), reveals a negative P_c value (-35%) around 1.96 eV, corresponding to the peak energy E_- of the semi-dark trion state $|E_-\rangle$, and a positive P_c (18%) around the position of E_+ , associated with the bright trion state $|E_+\rangle$.

This result is similar to that reported by Zhang et al. [3], on magnetic-field brightening of the dark (gray) exciton and trion in ML WSe₂. In their case, the brightened dark excitonic complexes exhibited negative P_c , i.e., $I(\sigma-) > I(\sigma+)$,

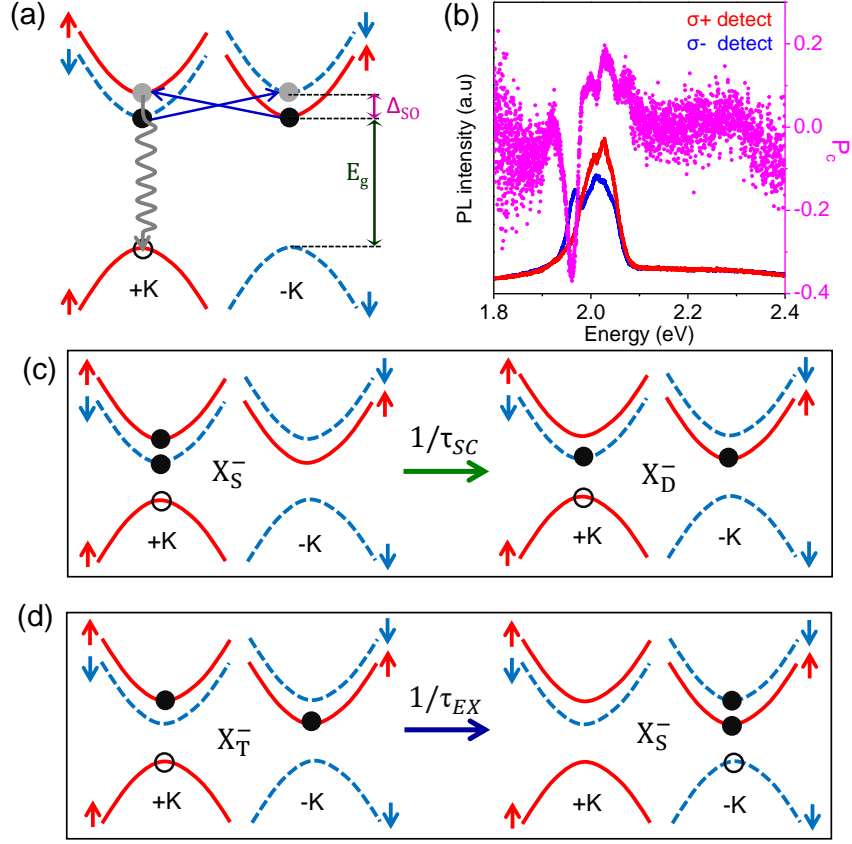


FIG. 4. Schematic diagram of the intervalley scattering processes that couple the dark and bright states of triions. E_g is the band gap and Δ_{SO} stands for the CB spin-splitting. (b) Circular polarization-resolved PL spectrum of ML WS₂ on disordered Si/SiO₂/Au substrate, as detected in the $\sigma+$ and $\sigma-$ channels on excitation by $\sigma+$ 488 nm (2.54 eV) laser irradiation. (c) Spin conserving scattering process from X_S^- to X_D^- . (d) Scattering from X_T^- to X_S^- via e-h exchange interaction.

in contrast to the case of bright states, where the PL emission is co-polarized with the laser excitation. Although the precise mechanism underlying the observation could not be specified, the relaxation of bright excitons to dark excitons through intervalley electron scattering was speculated to be a possible origin.

To explain the origin of the negative valley polarization, one needs to take into account the singlet and triplet bright triions as well as the dark triions. As suggested in a theoretical study by Fu et al. [31], the reversal of the valley polarization (VP) could arise from the conversions between the dark and bright triion states. The reversal of the VP studied by Fu [31] refers to the polarization of the singlet triion X_S^- (negative P_c) in contrast to that of the triplet triion X_T^- (positive P_c). The splitting of a bright triion peak in the PL spectrum into a pair of singlet (lower energy) and triplet triion peaks has been demonstrated experimentally for both WSe₂ and WS₂ MLs, with the magnitude of the splitting measured to be approximately 6–7 meV [28]. Experimental evidence for the negative P_c of the singlet triion X_S^- has been reported only for WSe₂ MLs [8].

Two dynamical processes play a dominant role in the interconversions between the triion states, as illustrated in Figs. 4(c,d). In the first process [Fig. 4(c)], X_S^- scatters into the dark triion X_D^- via spin-conserving transfer (rate given by $1/\tau_{SC}$) of an electron from the upper CB subband in the +K valley to the lower CB subband in the -K valley [32]. An explicit value of τ_{SC} has not been reported so far but, as pointed out in Refs [31–34], the transition from X_S^- to X_D^- turns out to be the most favorable process in the inter-conversions between the bright and dark triions [31–34]. This implies that the scattering rate $1/\tau_{SC}$ is much larger than the singlet triion recombination rate. In the second process [Fig. 4(d)], the excitonic e-h pair part of X_T^- in the +K valley is transferred (rate given by $1/\tau_{EX}$, $\tau_{EX} \sim 4$ ps at 13 K) to the -K valley, forming X_S^- [32]. This process is mediated through the e-h exchange coupling, which is known to provide an efficient channel for valley depolarization [31–33, 35, 36]. The other possible dynamical processes require spin flips, thermal activation or simultaneous transfers of three particles, which are considerably less efficient in bringing about valley depolarization [31–36].

To understand the valley population imbalance, we re-express the P_c as

$$P_c = \frac{N(+K) - N(-K)}{N(+K) + N(-K)}, \quad (4)$$

where $N(+K)$ and $N(-K)$ denote the numbers of singlet trions in the $+K$ and $-K$ valleys respectively. The dominant (minority) component of the semi-dark trion state $|E_- \rangle$ is the dark (bright) trion state. In this state, there is a spectral overlap of the bright trion state, and hence its singlet component (X_S^-), with the dark trion state (X_D^-). The dominance of the dark component implies a significant conversion of X_S^- to X_D^- in the $+K$ valley. Moreover, the e-h exchange coupling facilitates the conversion of X_T^- in the $+K$ valley to X_S^- in the $-K$ valley. Thus, the occupation number of X_S^- in the $-K$ valley exceeds that in the $+K$ valley, i.e., $N(-K) > N(+K)$. Given that the optical transitions from the $-K$ valley yield $\sigma-$ polarized emission, the PL signal is characterized by a negative value of P_c . In the bright trion state $|E_+ \rangle$, the dominant component comes from the bright trion itself while the dark trion is a minority constituent. Since the coupled state is predominantly bright, i.e., the proportion of dark states is small, the population transfer from X_S^- to X_D^- is suppressed, and the depletion of X_S^- from the $+K$ valley is not significant. Furthermore, the P_c of the bright trion component is positive resulting in a net positive value of P_c .

III. CONCLUSION

In conclusion, our study demonstrates the brightening of dark trions and the amplification of the PL emission intensity, over the temperature range of 83 K -115 K, in a WS_2 ML sample. The earlier experiments [25, 26] on ML WS_2 , carried out at considerably lower temperatures (5 K and 7 K), reported a distinct semi-dark trion (partially brightened dark trion) emission line in the PL spectrum, the origin of which lies in intervalley e-e scatterings [Fig. 4(a)]. The key prediction of the scattering mechanism, that the peak energy difference between the dark ($|D \rangle$) and semi-dark ($|E_- \rangle$) trions is of the order of, Δ_{SO} , the CB spin-orbit splitting, has been experimentally confirmed [6, 25, 26]. The four-component analysis of our PL doublet also reproduces the result. As reported in [27], the PL emission line from the semi-dark trion becomes weaker, losing visibility thereby, at elevated temperatures due to the thermal activation of the lowest-energy semi-dark trion to the higher-energy bright trion state. The inclusion of the rough Au film in our experiment, as a substrate component, extends the temperature range for the detection of the semi-dark trion through a significant amplification of the weak PL signal, apart from enhancing the PL signal from the bright trion, brightening the dark trion and doping the sample with electrons needed for trion formation, an alternative to electrostatic gating. To summarize, our experimental study illustrates how a combination of intervalley e-e scattering and plasmonic coupling enables the detection of the PL signal emissions from the different species of trions in ML WS_2 , at elevated temperatures. The quantitative estimates emerging from our study are consistent with experimental results. The experimental observation of a negative P_c around the PL emission energy E_- is explained on the basis of available experimental evidence on trion dynamics in tungsten-based TMD materials. Beyond WS_2 , our approach establishes a scalable strategy for optical access to dark excitonic complexes in two-dimensional semiconductors, giving rise to new possibilities for valleytronic and nanophotonic applications.

Supporting Information

Section I : Methods

ML WS₂ was mechanically exfoliated from a bulk crystal, sourced from Manchester Nanomaterials, using the scotch tape method, and subsequently transferred, in two separate processes, onto a Si/SiO₂ and a rough Si/SiO₂/Au substrate. The latter substrate was fabricated by the sputtering of Au on a Si/SiO₂ substrate in a vacuum physical vapor deposition growth chamber (pressure $\sim 10^{-3}$ Torr). All PL measurements were performed in a back-scattering geometry using a micro-Raman spectrometer (Horiba LabRAM HR, Jovin Yvon), equipped with 600 lines/mm grating and a Peltier-cooled CCD detector. Excitation was provided by an air-cooled continuous wave Argon-ion laser with a wavelength of 488 nm (2.54 eV), focused onto the sample using a 50X objective lens with a numerical aperture of 0.75. The excitation power was ~ 0.1 mW unless otherwise stated. A linear polarizer was used into the incident optics and a quarter-wave plate was added to both the incident and collection paths followed by a half wave plate along with a linear polarizer at the collection optics for circularly polarization resolved PL studies. Low-temperature PL spectra were recorded using a Linkam THMS600 temperature-controlled stage.

Section II : Room temperature PL spectra

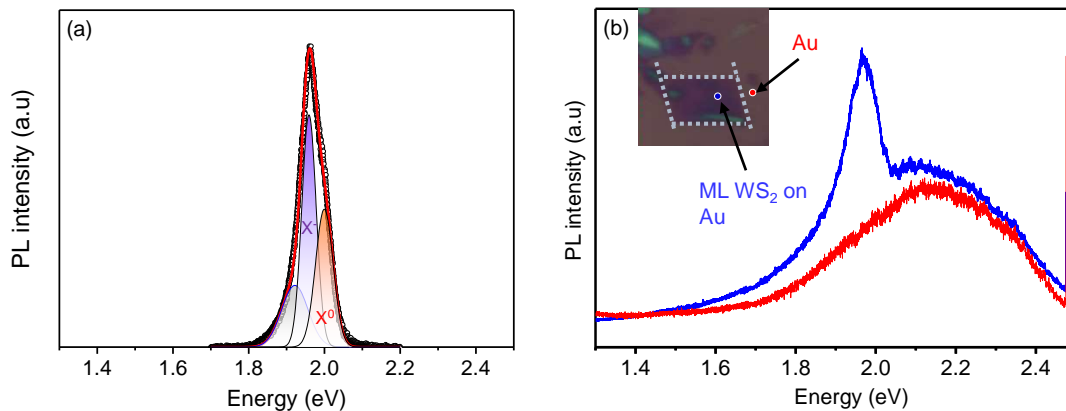


FIG. S1. (a) Room-temperature PL spectrum of ML WS₂ on a Si/SiO₂ substrate. (b) Room-temperature PL spectra from ML WS₂ on the disordered Au film and from the sole disordered Au film, as indicated in the figure.

Section III : Raman measurements

To evaluate the presence of strain in the sample, we performed Raman measurements at multiple positions across the sample at room temperature using a 100 \times objective with a numerical aperture (NA) of 0.9. Under these conditions, the laser spot size is approximately 660 nm, which is smaller than that used in the photoluminescence (PL) measurements (50 \times objective with NA = 0.75). Consequently, the Raman measurements provide higher spatial resolution than the PL measurements and are therefore more sensitive to local strain variations. The Raman spectra consistently show the characteristic E_{2g}¹ and A_{1g} modes at 357.5 cm⁻¹ and 421.4 cm⁻¹, respectively. Importantly, when Raman spectra were collected along a line scan spanning positions 1–3 [see Figure S2] across the sample, no measurable shift or broadening was observed in either Raman mode. Since the E_{2g}¹ mode is well known to be highly strain-sensitive, the absence of any detectable modulation in its peak position places a strict upper bound on strain in our sample [37–40]. Previous studies have shown that the E_{2g}¹ mode softens continuously under strain [37–40]. In contrast, our Raman data show neither softening nor broadening, indicating that the strain present in our sample is insignificant, which can affect exciton landscape.

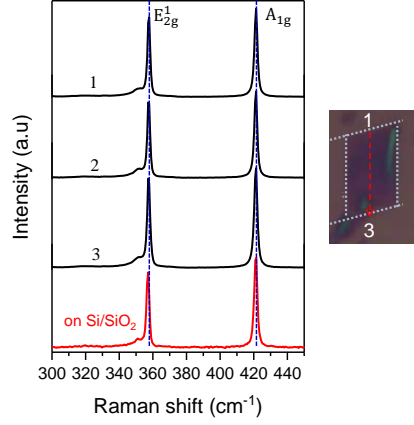


FIG. S2. Raman spectra acquired at multiple positions along the line scan on the ML WS₂ supported on the rough Au film (black curves). The right panel indicates the locations of the measurement points on the Au-supported sample. For comparison, the Raman spectrum from an ML WS₂ sample on a Si/SiO₂ substrate is also shown (red curve).

Section IV : Topography

We examined the local topography using AFM. The line-profile analysis in several regions (see Fig S3) of the sample reveals very small grain height variation. Such small topographic fluctuations are not expected to induce any appreciable strain in ML WS₂ [39].

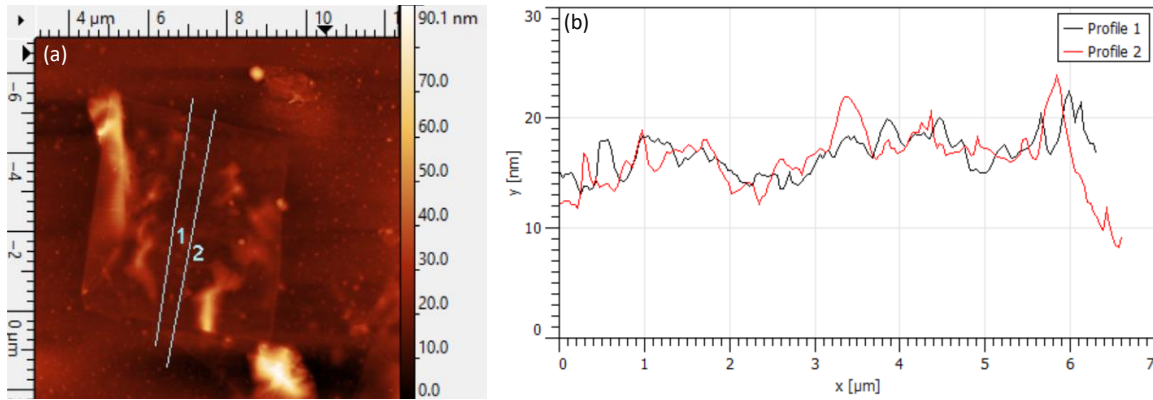


FIG. S3. (a) shows AFM image with different linescans (1,2), which are plotted in the right panel (b).

Section V : Laser power-dependent PL data

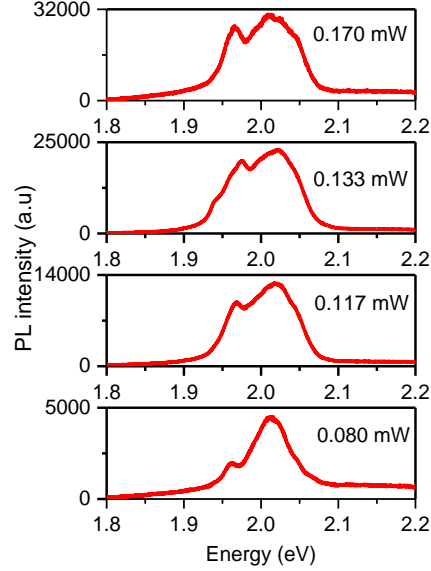


FIG. S4. (a) Laser power dependent PL spectra from ML WS₂ on a disordered Si/SiO₂/Au film at 83 K.

Section VI : Electrodynamics Simulation

To examine how the measured surface morphology of the Au film influences the spatial distribution of optical fields, we performed finite-element simulations using the experimentally obtained AFM height map as the input geometry. The AFM data were interpolated onto a two-dimensional computational mesh, and a frequency-domain wave equation was solved under plane-wave illumination using a scattered-field formulation.

Absorbing boundary conditions were applied at the outer edges of the simulation domain to minimize artificial reflections. The resulting field distributions were used to generate spatial maps of the out-of-plane near-field intensity above the surface, normalized to the incident field amplitude. These simulations are included to visualize morphology-dependent field localization and to support the discussion of enhanced radiative visibility of semi-dark trion on rough Au substrate.

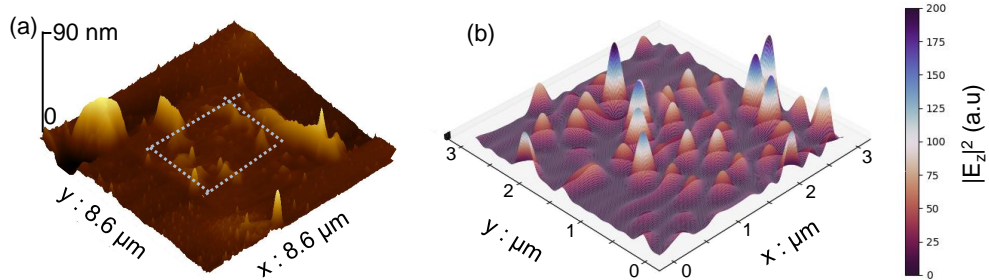


FIG. S5. (a) AFM image of the sample, where the dotted lines indicate central part of the sample, which has been taken for the simulation, result of which is shown in (b).

Section VII : Temperature-dependent PL spectra from ML WS₂ on disordered Si/SiO₂/Au substrate

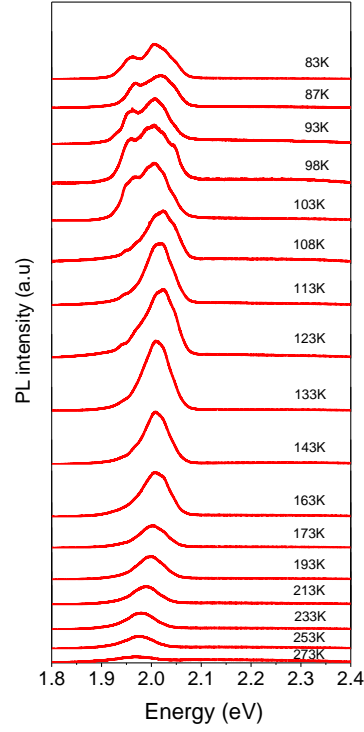


FIG. S6. (a) Temperature-dependent PL spectra from ML WS₂ on a disordered Si/SiO₂/Au film.

Section VIII : Integrated PL intensity as a function of temperature from ML WS₂ on Si/SiO₂ substrate

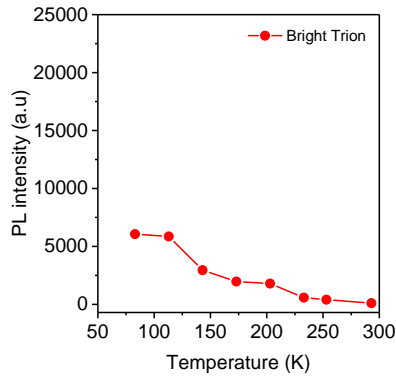


FIG. S7. Temperature-dependent integrated PL intensity of bright trion from ML WS₂ on a Si/SiO₂ substrate.

Section IX : Fine structure of PL spectrum from ML WS₂ on Si/SiO₂/Au substrate at 83 K

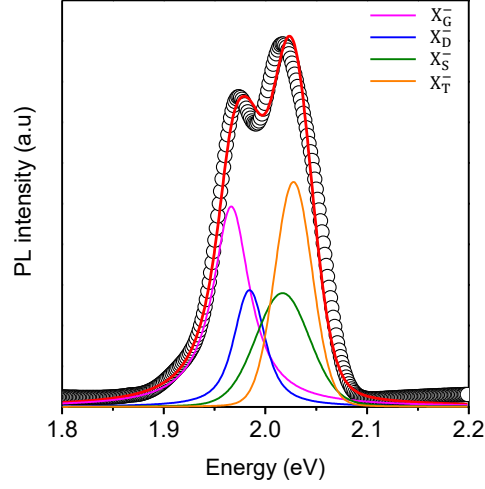


FIG. S8. Deconvoluted PL spectrum of monolayer WS₂ on a disordered Si/SiO₂/Au substrate at 83 K, resolved into four components corresponding to the semi-dark gray trion (X_G^-), the dark trion (X_D^-), the spin-singlet bright trion (X_S^-), and the spin-triplet bright trion (X_T^-). The fitted curve (red line) closely matches the experimental data set (open circles).

Section X : Circular polarization resolved PL spectra from ML WS₂ on Si/SiO₂ substrate at 83 K

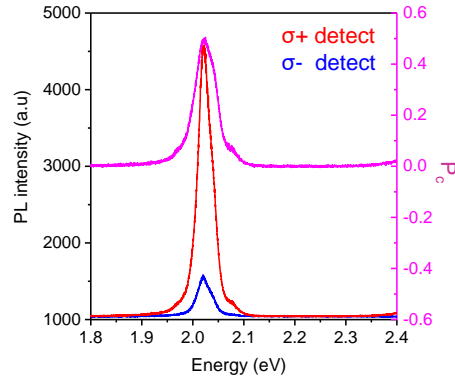


FIG. S9. Circularly polarization resolved PL spectra from a ML WS₂ on Si/SiO₂ substrate under $\sigma+$ circularly polarized excitation at 488 nm. Emission is analyzed in both $\sigma+$ and $\sigma-$ detection channels. The degree of circular polarization (P_c) is plotted as a function of emission energy. A P_c of approximately 50 % is observed for the bright trion emission and around 7 % for the bright neutral exciton.

-
- [1] J. R. Schaibley, H. Yu, G. Clark, P. Rivera, J. S. Ross, K. L. Seyler, W. Yao, and X. Xu, Valleytronics in 2D materials, Nat. Rev. Mater. **1**, 1 (2016).
 [2] X. Xu, W. Yao, D. Xiao, and T. F. Heinz, Spin and pseudospins in layered transition metal dichalcogenides, Nat. Phys. **10**, 343 (2014).

- [3] X.-X. Zhang, T. Cao, Z. Lu, Y.-C. Lin, F. Zhang, Y. Wang, Z. Li, J. C. Hone, J. A. Robinson, D. Smirnov, S. G. Louie, and T. F. Heinz, Magnetic brightening and control of dark excitons in monolayer WSe_2 , *Nat. Nanotechnol.* **12**, 883 (2017).
- [4] K.-D. Park, T. Jiang, G. Clark, X. Xu, and M. B. Raschke, Radiative control of dark excitons at room temperature by nano-optical antenna-tip Purcell effect, *Nat. Nanotechnol.* **13**, 59 (2018).
- [5] R. J. Gelly, D. Renaud, X. Liao, B. Pingault, S. Bogdanovic, G. Scuri, K. Watanabe, T. Taniguchi, B. Urbaszek, H. Park, and M. Lončar, Probing dark exciton navigation through a local strain landscape in a WSe_2 monolayer, *Nat. Commun.* **13**, 232 (2022).
- [6] V. Jindal, K. Mourzidis, A. Balocchi, C. Robert, P. Li, D. Van Tuan, L. Lombez, D. Lagarde, P. Renucci, T. Taniguchi, K. Watanabe, H. Dery, and X. Marie, Brightened emission of dark trions in transition metal dichalcogenide monolayers, *Phys. Rev. B* **111**, 155409 (2025).
- [7] Y. Zhou, G. Scuri, D. S. Wild, A. A. High, A. Dibos, L. A. Jauregui, C. Shu, K. De Greve, K. Pistunova, A. Y. Joe, T. Taniguchi, K. Watanabe, P. Kim, M. D. Lukin, and H. Park, Probing dark excitons in atomically thin semiconductors via near-field coupling to surface plasmon polaritons, *Nat. Nanotechnol.* **12**, 856 (2017).
- [8] C. Robert, S. Park, F. Cadiz, L. Lombez, L. Ren, H. Tornatzky, A. Rowe, D. Paget, F. Sirotti, M. Yang, D. Van Tuan, T. Taniguchi, B. Urbaszek, K. Watanabe, T. Amand, H. Dery, and X. Marie, Spin/valley pumping of resident electrons in WSe_2 and WS_2 monolayers, *Nat. Commun.* **12**, 5455 (2021).
- [9] E. Liu, J. van Baren, Z. Lu, M. M. Altairy, T. Taniguchi, K. Watanabe, D. Smirnov, and C. H. Lui, Gate Tunable Dark Trions in Monolayer WSe_2 , *Phys. Rev. Lett.* **123**, 027401 (2019).
- [10] X.-X. Zhang, Y. You, S. Y. F. Zhao, and T. F. Heinz, Experimental Evidence for Dark Excitons in Monolayer WSe_2 , *Phys. Rev. Lett.* **115**, 257403 (2015).
- [11] L. Ren, C. Robert, M. Glazov, M. Semina, T. Amand, L. Lombez, D. Lagarde, T. Taniguchi, K. Watanabe, and X. Marie, Control of the Bright-Dark Exciton Splitting Using the Lamb Shift in a Two-Dimensional Semiconductor, *Phys. Rev. Lett.* **131**, 116901 (2023).
- [12] L. Ren, L. Lombez, C. Robert, D. Beret, D. Lagarde, B. Urbaszek, P. Renucci, T. Taniguchi, K. Watanabe, S. A. Crooker, and X. Marie, Optical Detection of Long Electron Spin Transport Lengths in a Monolayer Semiconductor, *Phys. Rev. Lett.* **129**, 027402 (2022).
- [13] Y. Zhu, H. Jing, R.-W. Peng, C.-Y. Li, J. He, B. Xiong, and M. Wang, Realizing Anderson localization of surface plasmon polaritons and enhancing their interactions with excitons in 2D disordered nanostructures, *Appl. Phys. Lett.* **116**, 201106 (2020).
- [14] S. Grésillon, L. Aigouy, A. C. Boccarda, J. C. Rivoal, X. Quelin, C. Desmarest, P. Gadenne, V. A. Shubin, A. K. Sarychev, and V. M. Shalaev, Experimental observation of localized optical excitations in random metal-dielectric films, *Phys. Rev. Lett.* **82**, 4520 (1999).
- [15] M. Danovich, V. Zólyomi, and V. I. Fal'ko, Dark trions and biexcitons in WS_2 and WSe_2 made bright by e-e scattering, *Sci. Rep.* **7**, 45998 (2017).
- [16] B. N. Tugchin, N. Doolaard, A. I. Barreda, Z. Zhang, A. Romashkina, S. Fasold, I. Staude, F. Eilenberger, and T. Pertsch, Photoluminescence enhancement of monolayer WS_2 by n-doping with an optically excited gold disk, *Nano Lett.* **23**, 10848 (2023).
- [17] T. S. Bhattacharya, S. Mitra, S. S. Singha, P. K. Mondal, and A. Singha, Tailoring light-matter interaction in WS_2 -gold nanoparticles hybrid systems, *Phys. Rev. B* **100**, 235438 (2019).
- [18] J. Shi, J. Zhu, X. Wu, B. Zheng, J. Chen, X. Sui, S. Zhang, J. Shi, W. Du, Y. Zhong, Q. Wang, Q. Zhang, A. Pan, and X. Liu, Enhanced Trion Emission and Carrier Dynamics in Monolayer WS_2 Coupled with Plasmonic Nanocavity, *Adv. Opt. Mater.* **8**, 2001147 (2020).
- [19] C. Nayak, S. Masanta, S. Monga, S. Paul, S. Bera, S. Mondal, S. Bhattacharya, and A. Singha, Tailoring photoluminescence in MoSSe alloys through gold nanostructure coupling: Influence of midgap states and localized surface-plasmon resonance, *Phys. Rev. B* **109**, 125306 (2024).
- [20] T. S. Bhattacharya, S. Raha, P. K. Mondal, M. Pradhan, S. Ghosh, and A. Singha, Tuning light-matter interaction in 2D Bi_2Se_3 through plasmonic particle coupling, *Adv. Funct. Mater.* , e10990 (2025).
- [21] S. S. Singha, D. Nandi, and A. Singha, Tuning the photoluminescence and ultrasensitive trace detection properties of few-layer MoS_2 by decoration with gold nanoparticles, *RSC Adv.* **5**, 24188 (2015).
- [22] G. Moody, K. Tran, X. Lu, T. Autry, J. M. Fraser, R. P. Mirin, L. Yang, X. Li, and K. L. Silverman, Microsecond Valley Lifetime of Defect-Bound Excitons in Monolayer WSe_2 , *Phys. Rev. Lett.* **121**, 057403 (2018).
- [23] N. S. Mueller, R. Arul, G. Kang, A. P. Saunders, A. C. Johnson, A. Sánchez-Iglesias, S. Hu, L. A. Jakob, J. Bar-David, B. de Nijs, L. M. Liz-Marzán, F. Liu, and J. J. Baumberg, Photoluminescence upconversion in monolayer WSe_2 activated by plasmonic cavities through resonant excitation of dark excitons, *Nat. Commun.* **14**, 5726 (2023).
- [24] F. Fabbri, S. Raha, and F. Bianco, The interplay between neutral and charged excitons driven by electron irradiation in monolayer WSe_2 , *Materials Science in Semiconductor Processing* **191**, 109373 (2025).
- [25] M. Zinkiewicz, T. Woźniak, T. Kazimierzuk, P. Kapuscinski, K. Oreszczuk, M. Grzeszczuk, M. Bartoś, K. Nogajewski, K. Watanabe, T. Taniguchi, C. Faugeras, P. Kossacki, M. Potemski, A. Babiński, and M. R. Molas, Excitonic Complexes in n-Doped WS_2 Monolayer, *Nano Lett.* **21**, 2519 (2021).
- [26] S. B. Chand, J. M. Woods, J. Quan, E. Mejia, T. Taniguchi, K. Watanabe, A. Alù, and G. Grosso, Interaction-driven transport of dark excitons in 2D semiconductors with phonon-mediated optical readout, *Nat. Commun.* **14**, 3712 (2023).
- [27] J.-S. Tu, S. Borghardt, D. Grützmacher, and B. E. Kardynał, Experimental observation of a negative grey trion in an electron-rich WSe_2 monolayer, *J. Phys.: Condens. Matter* **31**, 415701 (2019).

- [28] G. Plechinger, P. Nagler, A. Arora, R. Schmidt, A. Chernikov, A. G. del Águila, P. C. Christianen, R. Bratschitsch, C. Schüller, and T. Korn, Trion fine structure and coupled spin–valley dynamics in monolayer tungsten disulfide, *Nat. Commun.* **7**, 12715 (2016).
- [29] L. Ren, C. Robert, H. Dery, M. He, P. Li, D. Van Tuan, P. Renucci, D. Lagarde, T. Taniguchi, K. Watanabe, X. Xu, and X. Marie, Measurement of the conduction band spin-orbit splitting in WSe₂ and WS₂ monolayers, *Phys. Rev. B* **107**, 245407 (2023).
- [30] P. Kapuściński, A. Delhomme, D. Vaclavkova, A. O. Slobodeniuk, M. Grzeszczyk, M. Bartos, K. Watanabe, T. Taniguchi, C. Faugeras, and M. Potemski, Rydberg series of dark excitons and the conduction band spin-orbit splitting in monolayer WSe₂, *Commun. Phys.* **4**, 186 (2021).
- [31] J. Fu, J. M. R. Cruz, and F. Qu, Valley dynamics of different trion species in monolayer WSe₂, *Appl. Phys. Lett.* **115**, 082101 (2019).
- [32] A. Singh, K. Tran, M. Kolarczyk, J. Seifert, Y. Wang, K. Hao, D. Pleskot, N. M. Gabor, S. Helmrich, N. Owschimikow, U. Woggon, and X. Li, Long-Lived Valley Polarization of Intravalley Trions in Monolayer WSe₂, *Phys. Rev. Lett.* **117**, 257402 (2016).
- [33] E. J. McCormick, M. J. Newburger, Y. K. Luo, K. M. McCreary, S. Singh, I. B. Martin, E. J. Cichewicz, B. T. Jonker, and R. K. Kawakami, Imaging spin dynamics in monolayer WS₂ by time-resolved kerr rotation microscopy, *2D Mater.* **5**, 011010 (2017).
- [34] F. Volmer, S. Pissinger, M. Ersfeld, S. Kuhlen, C. Stampfer, and B. Beschoten, Intervalley dark trion states with spin lifetimes of 150 ns in WSe₂, *Phys. Rev. B* **95**, 235408 (2017).
- [35] D. Vaclavkova, J. Wyzula, K. Nogajewski, M. Bartos, A. O. Slobodeniuk, C. Faugeras, M. Potemski, and M. R. Molas, Singlet and triplet trions in WS₂ monolayer encapsulated in hexagonal boron nitride, *Nanotechnology* **29**, 325705 (2018).
- [36] T. P. Lyons, S. Dufferwiel, M. Brooks, F. Withers, T. Taniguchi, K. Watanabe, K. Novoselov, G. Burkard, and A. I. Tartakovskii, The valley zeeman effect in inter-and intra-valley trions in monolayer WSe₂, *Nat. Commun.* **10**, 2330 (2019).
- [37] Y. Wang, C. Cong, W. Yang, J. Shang, N. Peimyoo, Y. Chen, J. Kang, J. Wang, W. Huang, and T. Yu, Strain-induced direct–indirect bandgap transition and phonon modulation in monolayer WS₂, *Nano Research* **8**, 2562 (2015).
- [38] F. Wang, S. Li, M. A. Bissett, I. A. Kinloch, Z. Li, and R. J. Young, Strain engineering in monolayer WS₂ and WS₂ nanocomposites, *2D Materials* **7**, 045022 (2020).
- [39] E. Blundo, M. Felici, T. Yildirim, G. Pettinari, D. Tedeschi, A. Miriametro, B. Liu, W. Ma, Y. Lu, and A. Polimeni, Evidence of the direct-to-indirect band gap transition in strained two-dimensional WS₂, MoS₂, and WSe₂, *Physical Review Research* **2**, 012024 (2020).
- [40] A. Michail, D. Anestopoulos, N. Delikoukos, S. Grammatikopoulos, S. A. Tsirkas, N. N. Lathiotakis, O. Frank, K. Filintoglou, J. Parthenios, and K. Papagelis, Tuning the photoluminescence and raman response of single-layer WS₂ crystals using biaxial strain, *The Journal of Physical Chemistry C* **127**, 3506 (2023).

ACKNOWLEDGMENTS

I.B. acknowledges the support of NASI, Allahabad, India, under the Honorary Scientist Scheme. A.S. thanks the Science and Engineering Research Board (SERB), India, for their financial support (File No. EMR/2017/002107). The authors acknowledge the assistance of Suvadip Masanta, Chumki Nayak, Pritam Sinha, Subhajit Mahapatra, and Prithwiraj Majhi. The authors thank the Central Instrumental Facility at S. N. Bose National Centre for Basic Sciences (SNBNCBS), Kolkata, for assisting with the AFM measurements. The authors thank Prof. Xavier Marie for useful discussions.